K. J. Myers
Associate Professor.

R. W. Ward
Graduate Student.

Chemical and Materials Engineering,
University of Dayton,
Dayton, OH 45469-0246

André Bakker
Technical Director,
Chemineer, Inc.,
Dayton, OH 45401-1123

A Digital Particle Image Velocimetry Investigation of Flow Field Instabilities of Axial-Flow Impellers

Digital particle image velocimetry (DPIV) has been used to examine the flow field in a vessel agitated by an axial-flow impeller in turbulent operation. Both a pitched-blade turbine and a high-efficiency impeller were studied. Time series analysis indicates that the flow field is not steady; rather, it is subject to transients with frequencies well below the blade passage frequency (periods ranging from 40 to over 300 impeller revolutions have been observed). This result has important implications for computational modeling because current descriptions of agitated vessels are based upon time-averaged flow fields with superimposed turbulence. This modeling approach may not accurately capture the mixing associated with the low-frequency phenomena observed in this study.

Introduction

Mechanically agitated vessels are in widespread use in the chemical processing and allied industries. Their diverse array of applications includes storage tanks, blending operations, crystallization, fermentation, and as chemical reactors. Design of agitators has traditionally relied on qualitative rules of thumb and past experience. However, with the increasing availability of enhanced computational and experimental techniques, there is a growing emphasis on understanding the fundamentals of agitated vessel performance. In many instances the success or failure of an agitator can be directly related to the flow in the vessel and how it impacts physical and chemical transformations.

It is becoming apparent that the flow fields in agitated vessels are not invariant. Rather, they are influenced by Reynolds number (Wang et al., 1995) and geometry (Kresta and Wood, 1993). Further, there is growing evidence that the flow fields produced by axial-flow impellers are time-dependent, exhibiting transients with frequencies considerably less than those associated with small-scale turbulence and blade passage. In this work, digital particle image velocimetry (DPIV) is used to characterize low frequency transients in the flow fields produced by axial-flow impellers.

Studies of Flow Pattern Instability

Numerous recent publications have demonstrated that the flow field produced by an axial-flow impeller is not truly steady, but rather is subject to instabilities with time scales that are substantially longer than those associated with blade passage and small-scale turbulence. Single-phase flow patterns of various axial-flow impellers have been studied by several methods. Chapple and Kresta (1993) used tuft visualization to study the stability of the flow patterns produced by a three-blade hydrofoil impeller and a pitched-blade turbine. They also characterized the influence of geometric parameters such as impeller off-bottom clearance, impeller diameter, and number of baffles on flow pattern stability. Brůha et al. (1994, 1995) identified time dependence in the flow pattern of a pitched-blade turbine using a mechanical measuring device. They found that the frequency of transition in the flow pattern is linearly related to the speed of impeller rotation, but is much slower than the speed of impeller rotation. Winardi and Nagase (1991) used a combination of flow visualization techniques to examine the flow patterns produced by a marine propeller. They described the observed flow patterns as quick return, full circulation, and intermediate circulation. They measured the lifetime distribution of these patterns and found that the flow pattern changes were random in their order and that the lifetime of a given flow pattern could range from half a second to several minutes. Using laser Doppler velocimetry (LDV) Bakker and Van den Akker (1994a) found that in the upper portions of a vessel agitated by a pitched-blade turbine the axial velocity exhibited bimodal and trimodal distributions. This behavior suggests that the flow in this region is not stable, perhaps oscillating between a number of quasi-stable flows.

A few process-oriented investigations have also indicated the unstable nature of the flow patterns produced by axial-flow impellers. Haam et al. (1992) found that the magnitude of the interphase (vessel to inside wall) heat transfer coefficient in an agitated vessel is periodic in nature. They attributed the oscillations in the heat transfer coefficient to the slow (relative to the impeller speed) precession of an axial vortex around the vessel. Bakker and Van den Akker (1994b) observed periodic fluctuations in the local gas holdup for systems agitated with axial-flow impellers. Again, the frequency of the fluctuations were slow relative to the speed of impeller rotation. As in Haam et al.'s heat transfer study, this behavior was attributed to an asymmetric flow pattern caused by complex nonstationary vortex motion. Thus, both fundamental and process studies have established the unstable nature of the flow fields produced by axial-flow impellers. The observed instabilities have exhibited a wide range of frequencies, with many instabilities occurring over a time scale much longer than that associated with impeller rotation or blade passage. However, characterization of these instabilities is incomplete and very little is known about their origin and influence on mixing performance.

The DPIV Technique

Digital particle image velocimetry (DPIV) combines the optical flow characterization technique of particle image velocime-

Contributed by the Fluids Engineering Division for publication in the JOURNAL OF FLUIDS ENGINEERING. Manuscript received by the Fluids Engineering Division April 2, 1996; revised manuscript received December 5, 1996. Associate Technical Editor: P. W. Bearman.

try (PIV) with digital image processing to yield a rapid, nonintrusive method to study flow fields. Like many other velocimetry techniques, DPIV requires seeding the flow with particles that mimic the motion of the liquid. In the case of DPIV, these particles fluoresce when exposed to light of a characteristic wavelength. This light is provided by a laser whose output is manipulated into a light sheet that illuminates a plane of the flow field to be studied. To increase processing speed, rather than using photographic techniques, DPIV captures the images of the fluorescent particles digitally with a charge coupled device (CCD) camera.

To obtain fluid velocities, two images of the seeded flow field are captured digitally at successive points in time, and comparison of these images allows the velocity field in the system to be constructed. To do this, the flow field is divided into smaller interrogation regions that are considered individually. Rather than tracking individual particles, cross correlation is used to obtain the average particle displacement of the ensemble of particles in an interrogation region from the successive flow field images. Computationally, cross correlation is achieved with two-dimensional signal processing techniques whose speed is enhanced through the use of fast Fourier transforms. The fluid velocity is then calculated assuming linear displacement over the time interval between the successive images.

Willert and Gharib (1991) have described DPIV in greater detail, focusing on the cross correlation technique and its implementation. The accuracy of DPIV relies on experimentation under appropriate conditions. These include a minimum particle displacement of two particle diameters, a maximum particle displacement of twenty-five percent of the interrogation region dimension, minimal out-of-plane displacement, and a minimum of five particles in an interrogation region to ensure accurate velocity measurements.

Experimental Apparatus and Procedures

The DPIV apparatus used in this study is a commercial system acquired from Dantec Measurement Technology. Figure 1 illustrates the primary components of the apparatus. A continuous argon-ion laser is the light source. A light sheet probe equipped with a prism converts the beam into a nominal 0.01 meter thick light sheet. Background laser reflections are virtually eliminated with an optical cutoff filter. The thick light sheet used in this study reduces the effects of tangential motion that carries particles in and out of the plane of study. This effect is particularly significant in the impeller region where the tangential velocities are higher than in the rest of the vessel. The flow is seeded with approximately 5000 80-micron diameter fluorescent spheres in the illuminated plane. The CCD camera is placed 1.8 m from the plane of the light sheet. Placement of the CCD camera far from the plane of study minimizes errors in determination of the axial and radial velocities due to tangential movement of particles within the rather thick light sheet. The CCD camera captures a 512 by 480 pixel image of the flow field. This image is divided into either 16 by 16 or 32 by 32 pixel interrogation regions, depending on the expected velocities. An 8 pixel step size between adjacent interrogation regions is used, resulting in fifty percent or seventy-five percent overlap, respectively. The two-dimensional DPIV flow field is then represented by a discrete flow field containing approximately 3000 velocity vectors. Oversampling the velocity field by overlapping the interrogation regions provides more velocity vectors which aids in the removal of velocity outliers, reinterpolation, and smoothing of the velocity field, all of which improve the accuracy of the measurements.

The diameter of the cylindrical, flat-bottomed plexiglass vessel used in this work was 0.292 meters. This vessel was placed in a square plexiglass tank filled with water to reduce optical distortion. The vessel was equipped with four vertical baffles that were evenly spaced about the periphery of the vessel. The baffle widths were equal to one-twelfth of the vessel diameter. The baffles were offset from the vessel wall by a distance equal to one-sixth of the baffle width. The liquid used was water and the liquid level was equal to the tank diameter ($H/T = 1$). The three-dimensional, cylindrical vessel could be rotated relative to the laser light sheet so that data could be taken in any vertical plane. For some experiments the plane of study was located midway between the baffles, while for other experiments a plane slightly in front of the plane between two baffles was studied

Two impellers were studied (refer to Fig. 1). The first was the P-4, a four-bladed, forty-five degree pitched-blade turbine with a diameter of 0.102 meters ($D/T = 0.35$). The width of the impeller blades was one-fifth of the impeller diameter ($W/D = 0.20$). This impeller was studied at off-bottom clearances of 0.134 meters ($C/T = 0.46$, $C/D = 1.31$) and 0.097 meters ($C/T = 0.33$, $C/D = 0.94$). The second impeller studied was

Nomenclature

C = impeller off-bottom clearance, measured from the lowest point on the impeller to the vessel base (m)
D = impeller diameter (m)
f, f_1 = frequency of large-scale flow pattern fluctuations (s^{-1})
H = total liquid depth (m)
N = agitation speed (revolutions per second, s^{-1})
$P(f_1)$ = power spectral density of the spatially-averaged vorticity-time record (−)
S = ratio of velocity standard deviation to time-averaged velocity (−)
t = time (s)
T = vessel diameter (m)
u = velocity in the x-direction (m/s)
v = velocity in the y-direction (m/s)
$\mathbf{v}$ = velocity vector (m/s)
W = impeller blade width (m)
W_1 = discrete Fourier transform of the spatially-averaged vorticity-time record (−)
y = distance above the vessel base (m)
ν = kinematic viscosity (m^2/s)
σ = standard deviation in the velocity (m/s)
$\boldsymbol{\omega}$ = vorticity vector (s^{-1})

Subscripts

i = index for x-direction (−)
I = total number of interrogation regions in the x-direction (−)
j = index for y-direction (−)
J = total number of interrogation regions in the y-direction (−)
k = flow field number in the time series (−)
K = total number of flow fields in the time series (−)
1 = frequency index
z = indicates z coordinate (−)

Operators

∇ = vector differential operator (m^{-1})
X = vector cross product operator (−)
Σ = summation operator (−)
$\langle\ \rangle$ = area average operator (−)
$\overline{\ }$ = time average operator (−)
Δ = difference operator (−)

Acronyms

CCD = charge coupled device
DPIV = digital particle image velocimetry
LDV = laser Doppler velocimetry
PIV = particle image velocimetry
PSD = power spectral density

Figure 1 (top)

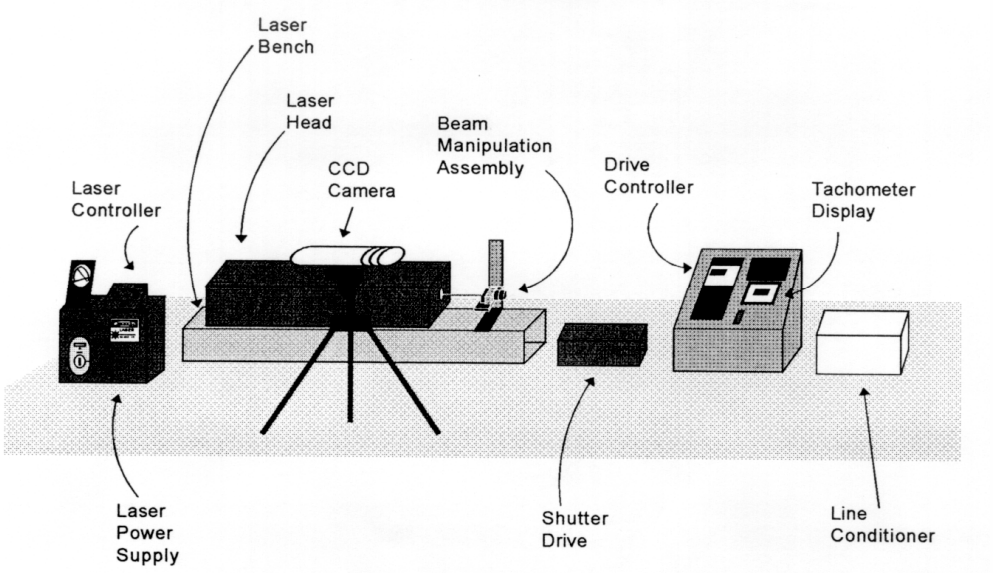

Figure 1 (middle)

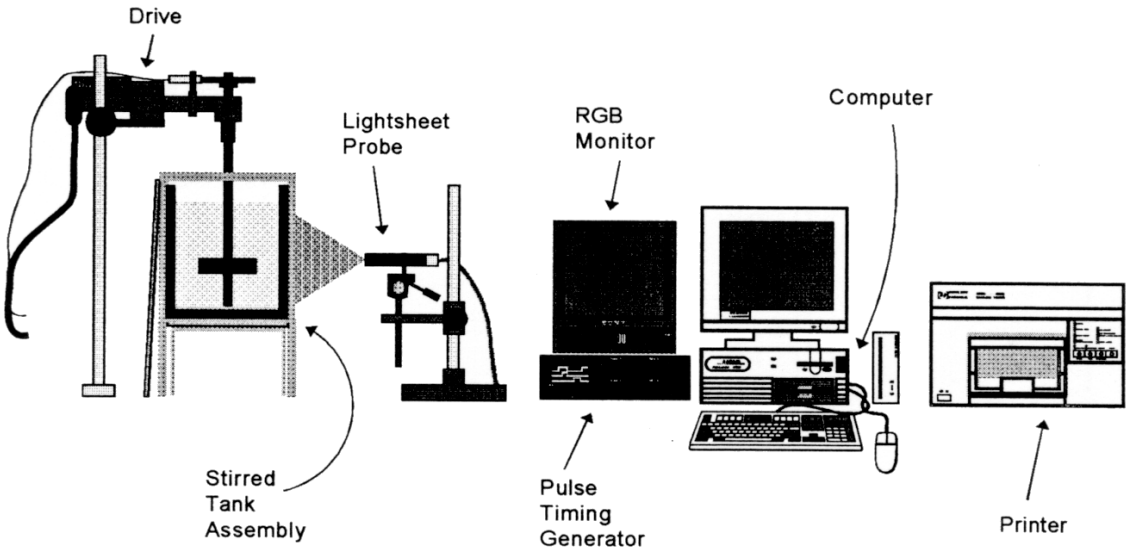

Figure 1 (bottom)

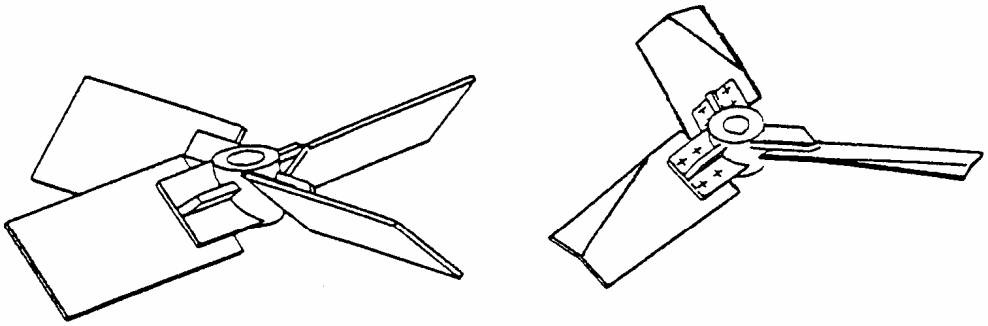

Fig. 1 Experimental apparatus: laser, controls, and CCD camera (top), vessel and computing hardware (center), and impellers studied (bottom)

a high-efficiency impeller, a Chemineer HE-3 of standard construction with a diameter of 0.114 meters ($D/T = 0.39$). This impeller was studied only at an off-bottom clearance of 0.097 meters ($C/T = 0.33$, $C/D = 0.84$). Operation at speeds of either 0.6 or 1 s^{-1} (36 or 60 rpm) yielded impeller Reynolds numbers (ND^2/ν) ranging from 6,190 to 13,100, the lower end of the turbulent regime.

The successive images for DPIV analysis were captured using a time delay of 0.033 seconds between the images (this corresponds to the standard video timing rate). This delay was appropriate for the relatively low velocities encountered in this work. The highest impeller tip speed used was 0.36 m/s, and the maximum fluid velocities would be only a fraction of this value. Further, a series of image pairs was taken to study the transient behavior of the flow field. Series of either 64 or 1024 image pairs were taken. The successive image pairs were separated by a time delay of approximately 11 seconds for the 64 image pair series and 1.3 seconds for the 1024 image pairs series. This yielded time records of 700 or 1330 seconds (11.7 or 22.2 minutes). Time series analysis was performed only on the data sets obtained with the faster sampling rate (with a delay of 1.3 seconds between successive image pairs). Since this sampling rate is approximately 30 times faster than the fastest transients observed in the flow field, aliasing errors are not likely to be significant. To further verify that aliasing did not influence the results and that the observed changes in flow pattern were not associated with blade passage, a set separate of experiments was performed. These experiments used a much shorter time delay of 0.167 seconds between successive image pairs. These results are discussed in the section Blade Passage Effects.

Data Analysis

Computational options following measurement of the series of two-dimensional velocity fields include calculation of the time-averaged velocity field, calculation of quantities such as vorticity and the standard deviation in the velocity, and the construction of one-dimensional time series.

The time-averaged velocity components at a point i, j in the flow field are calculated in the following manner.

$$\bar{u}_{i,j} = \frac{1}{K}\sum_{k=1}^{K} u_{i,j,k} \quad \bar{v}_{i,j} = \frac{1}{K}\sum_{k=1}^{K} v_{i,j,k} \tag{1}$$

Here u and v are the velocities in the x-direction and the y-direction, respectively, i and j denote the x and y locations in the flow field, k denotes the kth flow field in the time series, and K is the total number of near-instantaneous flow fields measured. Note that the cylindrical coordinates, with radial, tangential, and axial components, typically used to describe flow in agitated vessels have been replaced by a planar coordinate system since the DPIV technique provides a near-instantaneous, two-dimensional flow field in the plane illuminated by the laser light sheet. In this planar coordinate system, the x coordinate replaces the radial coordinate and the y coordinate replaces the axial coordinate (with the y position measured relative to the base of the vessel). The z coordinate, which will be important relative to the calculation of vorticity, is normal to the illuminated plane of study.

The standard deviation in the velocity at any point in the flow field, $\sigma_{i,j}$, can also be calculated.

$$\sigma_{i,j} = \sqrt{\frac{1}{K}\sum_{k=1}^{K}(u_{i,j,k}^2 + v_{i,j,k}^2) - \frac{1}{K^2}\left(\sum_{k=1}^{K}(u_{i,j,k}^2 + v_{i,j,k}^2)^{1/2}\right)^2} \tag{2}$$

This velocity standard deviation is a measure of the energy contained in the fluctuating velocities in the flow field. The ratio of the standard deviation and the magnitude of the average velocity, often termed the coefficient of variation,

$$S_{i,j} = \frac{\sigma_{i,j}}{\sqrt{\bar{u}_{i,j}^2 + \bar{v}_{i,j}^2}} \tag{3}$$

provides an indication of the local stability of the flow.

Vorticity is the curl of the velocity vector ($\boldsymbol{\omega} = \nabla \times \mathbf{v}$) and characterizes the rotation of fluid elements in the flow field. Vorticity is a vector with a characteristic direction normal to the plane in which rotation occurs (as determined by the right hand rule). For a two-dimensional flow field such as that obtained by DPIV, this directional aspect can simply be described by the sense (sign) of the vorticity. Positive vorticity (directed out of the plane of observation) corresponds to counterclockwise rotation while negative vorticity (directed into the plane of observation) corresponds to clockwise rotation. Given a near-instantaneous, two-dimensional (x-y) velocity field at time step k, the z-component of vorticity at the point i, j in the flow field

$$(\omega_{i,j,k})_z = \frac{\partial v_{i,j,k}}{\partial x} - \frac{\partial u_{i,j,k}}{\partial y} \tag{4}$$

can be calculated from the discrete velocity fields using finite difference approximations of the derivatives. The spatially-averaged vorticity of the kth near-instantaneous velocity field, $\langle\omega\rangle_k$, is calculated as follows.

$$\langle\omega\rangle_k = \frac{1}{I \cdot J}\sum_{i=1}^{I}\sum_{j=1}^{J}(\omega_{i,j,k})_z \tag{5}$$

This yields a one-dimensional time series of the spatially-averaged vorticity of the near-instantaneous velocity fields. As will be seen, the spatially-averaged vorticities of near-symmetric flow fields are approximately zero, while the spatially-averaged vorticities of asymmetric flow fields have large magnitudes. A high positive spatially-averaged vorticity indicates that there are more (or larger) counterclockwise circulation loops, while a high negative spatially-averaged vorticity indicates that there are more (or larger) clockwise circulation loops.

The time series of the spatially-averaged vorticity is then further analyzed by calculating the power spectral density function (PSD), $P(f_1)$, which identifies the dominant frequencie of the time series. The power spectral density is determine from the discrete Fourier transform of the spatially-averaged vorticity, W_1.

$$W_1 = \sum_{k=0}^{K-1}\langle\omega\rangle_k e^{2\pi ikl/K} \quad l = 0, \ldots, K-1 \tag{6}$$

$$P(f_1) = \frac{1}{K^2}[|W_l|^2 + |W_{K-l}|^2]$$

$$l = 1, 2, \ldots, \left(\frac{K}{2} - 1\right) \quad f_1 = \frac{1}{K\Delta t} \tag{7}$$

f_1 represents frequency (note that $i^2 = -1$ in Eq. (6), not the x-direction index as in other equations). The discrete Fourier transform is calculated using a fast Fourier transform (FFT) algorithm after applying a Welch window to the time series of $\langle\omega\rangle_k$. These algorithms are described by Press et al. (1992).

Comparison of DPIV and LDV Data

Since the DPIV technique has not been previously used to study flow fields in agitated vessels, a comparison between DPIV and a more traditional measurement technique is warranted. Figure 2 compares the time-averaged (over the series of 64 image pairs) DPIV flow field with the LDV flow field reported by Lee (1994). Lee's data was taken in a 0.145-meter diameter vessel, and all length ratios (D/T, C/T, H/T, etc.) were approximately equal to those of this study. The DPIV flow field was obtained at a speed of 0.6 s^{-1} (36 rpm; impeller Reynolds number of 6,190), while Lee's data was taken at a speed of 8.33 s^{-1} (500 rpm; impeller Reynolds number of 21,500). The LDV data was taken in the plane of two baffles. Since light scattering by the baffles prevents data acquisition in

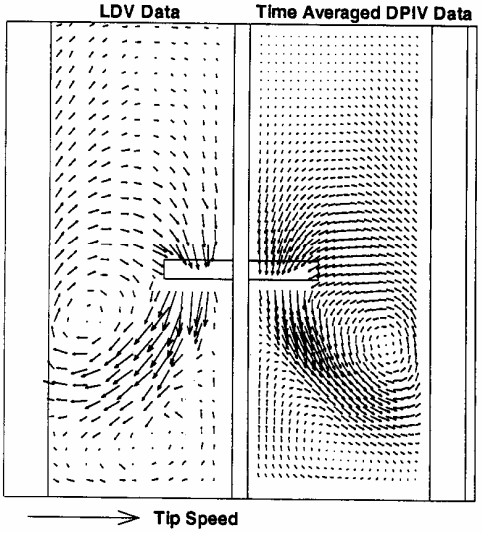

Fig. 2 Comparison of the normalized time-averaged velocity fields of a pitched-blade turbine as determined by LDV (left) and DPIV (right)

the baffle plane, DPIV data was taken directly in front and behind the baffle plane and averaged to yield an approximation of the baffle plane behavior. Both flow fields of Fig. 2 have been normalized with respect to impeller tip speed to account for the differences between the absolute velocities of the two experimental systems. The areas of the flow fields have also been scaled to the same size for this side-by-side comparison.

The two flow fields of Fig. 2 demonstrate good qualitative agreement between the DPIV and LDV measurement techniques. Previously, Fasano and Bakker (1993) have shown that the velocity fields determined by PIV are comparable to those predicted by computational fluid mixing simulation with LDV-prescribed impeller boundary conditions. The highest velocities in both flow fields are in the impeller outflow which has a relatively large radial velocity component. This flow impinges on the vessel wall which leads to reversed (radially inward) flow at the base of the vessel. Thus, the overall flow field can be described as a double figure eight, with flow loops beside and below the impeller. One qualitative difference between the two flow fields is the location of the centers of the circulation loops. This may be due to small differences in the geometries of the two experimental systems. In particular, the DPIV vessel of this study had a small gap between the wall and the baffles, while the vessel of Lee's LDV study used baffles that were flush with the wall.

Figure 3 is a more quantitative comparison of the axial and radial velocities measured by the DPIV and LDV techniques. Again, all velocities are normalized with respect to impeller tip speed. y represents the distance between the measurement point and the base of the vessel, and H represents the total liquid height. Also, negative axial velocities are directed downwards in the vessel. Although there are differences in the velocities determined by the two techniques, the quantitative agreement is reasonable except for the highest velocities in the impeller outflow region ($y/H = 0.4$). The magnitudes of these highest velocities are greater for LDV than for DPIV. The lower velocities of DPIV may be due to out-of-plane movement of the fastest particles caused by the tangential flow in the impeller discharge. Also, the LDV technique may have a bias towards higher velocities since during a certain time period more particles will pass through the measurement volume if the velocity is high than when the velocity is low (Lee, 1994).

The accuracy of the DPIV data in the impeller outflow region can be improved by limiting the effect of out-of-plane particle displacement by using shorter time delays between the two digital images that are used to construct the flow field. However, this leads to inaccuracies in measuring the lower velocities outside of the impeller outflow region because the small displacements of these particles would not be accurately measured given the spatial resolution of the digital technique. Since the entire flow field is required for the following instability analysis, a compromise is necessary. However, given the differences observed between the LDV and DPIV techniques, a direct comparison of these methods on the same agitated vessel is warranted (recall that two different vessels were used in the present comparison).

DPIV Study of Flow Instability

The DPIV flow pattern shown in Fig. 2 is the average of 64 near-instantaneous flow fields taken over a period of 700 seconds (11.7 minutes). The DPIV flow pattern and that found by LDV are clearly very similar. However, as shown in Fig. 4, the near-instantaneous flow fields determined by DPIV are more complex than the time-averaged flow field of Fig. 2. In general, any near-instantaneous flow field may look very little like the time-averaged flow field. The following study of flow pattern instability was performed at a speed of 1 s^{-1} (60 rpm), with

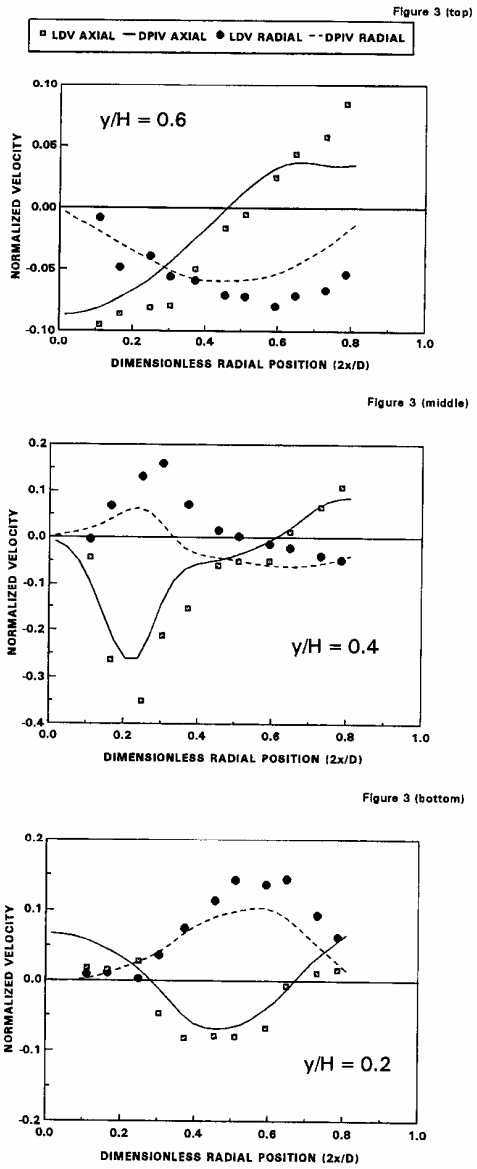

Fig. 3 Comparison of LDV and DPIV normalized time-averaged velocities: $y/H = 0.6$ (top), $y/H = 0.4$ (center), and $y/H = 0.2$ (bottom)

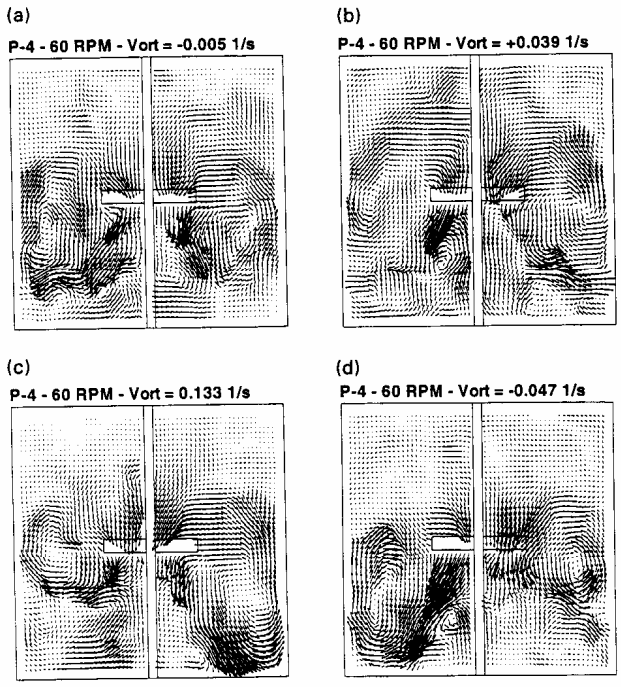

Fig. 4 Near-instantaneous DPIV velocity fields: (*a*) symmetric; (*b*) near symmetric with less structure; (*c*) and (*d*) asymmetric

the plane of study being located midway between the baffles for the pitched-blade turbine and slightly in front of the baffle plane for the HE-3 impeller. A series of 1024 near-instantaneous flow fields was obtained over a period of 1330 seconds (22.2 minutes). The instability of the flow field introduces the problem of analyzing this transient phenomenon, and a number of approaches were considered.

The spatially-averaged velocity in the plane of study was found to fluctuate with time, with some fluctuations being greater than ten percent of the mean (time-averaged) velocity. Figure 5 presents the standard deviation of velocity, σ, and the ratio of the velocity standard deviation to the time-averaged velocity, S (again with the pitched-blade turbine at $C/T = 0.46$; the corresponding time-averaged DPIV velocity field was previously presented in Fig. 2). The standard deviation of velocity can be seen to be largest in the impeller outflow. However, since the velocities are also high in this region, the relative instability of the flow (as expressed by the ratio of the velocity standard deviation to the time-averaged velocity) is rather low in this region. There are three regions of the flow field that are particularly unstable. The first region is near the liquid surface where the velocities are very low and the flow direction is not well-defined (i.e., the flow changes direction, typically being directed radially-inward, but sometimes being directed radially-outward). A second region of flow instability is the center of rotation in the upper flow loop of the flow field. Although the standard deviation of velocity is low in this region, the velocities are also low. This, and the mobile nature of the center of rotation make this region unstable. The third region of instability is the boundary between the upper and lower flow loops, including the region where the wall meets the base of the vessel. The velocities in this region are high, indicating that the boundary between the flow loops is mobile, similar to the center of rotation of the upper flow loop.

The parameter that yielded the best analysis of the transient flow field was vorticity. Figure 6 is a plot of the vorticity field associated with the time-averaged DPIV velocity field of Fig. 2 (the pitched-blade turbine with $C/T = 0.46$). This field has four regions of high vorticity. The discharge flow to the right of the impeller rotates counterclockwise, and therefore has a

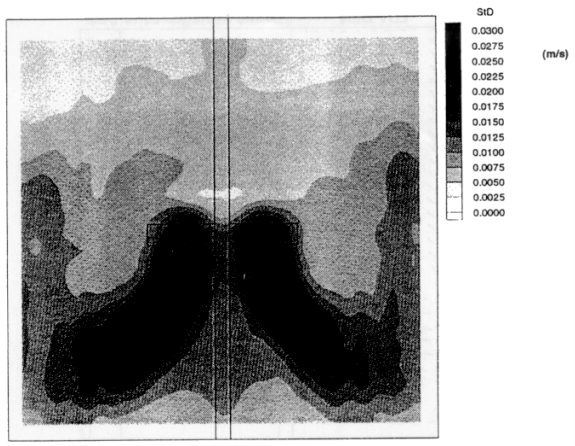

Fig. 5(*a*) Velocity standard deviation of the pitched-blade turbine

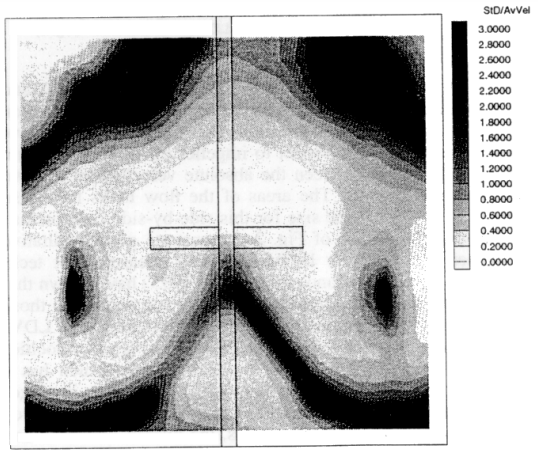

Fig. 5(*b*) Ratio of the velocity standard deviation to the time-averaged velocity of the pitched-blade turbine

positive vorticity. Conversely, the discharge flow to the left of the impeller rotates clockwise and has a negative vorticity. The flows returning to the impeller from below also have high vorticity. The flow to the right rotates clockwise and has a negative

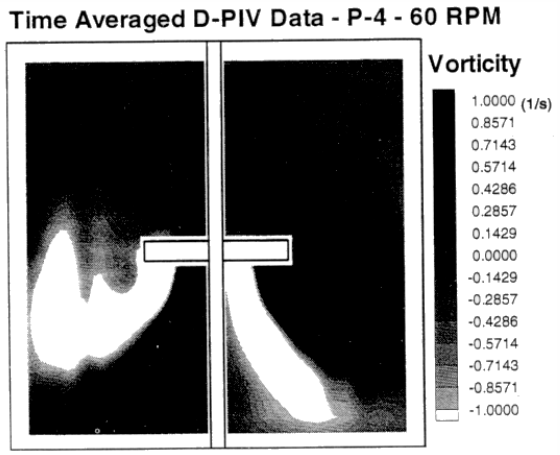

Fig. 6 Vorticity field corresponding to the time-averaged DPIV velocity field of Fig. 2

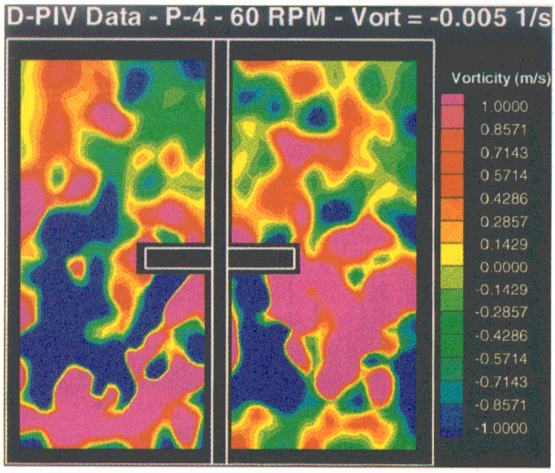

Fig. 7(*a*)

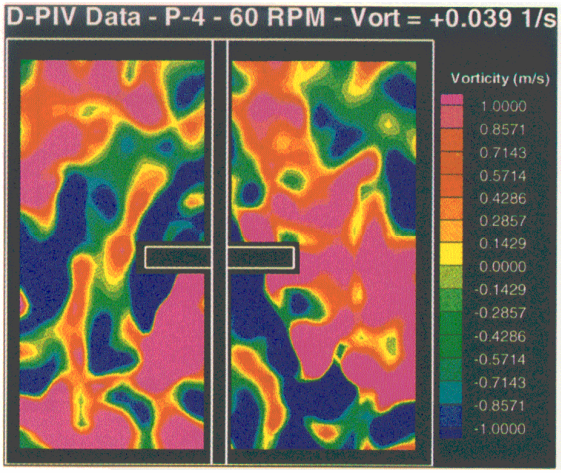

Fig. 7(*b*)

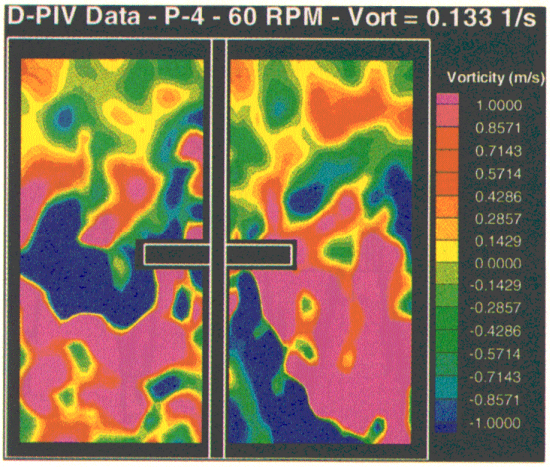

Fig. 7(*c*)

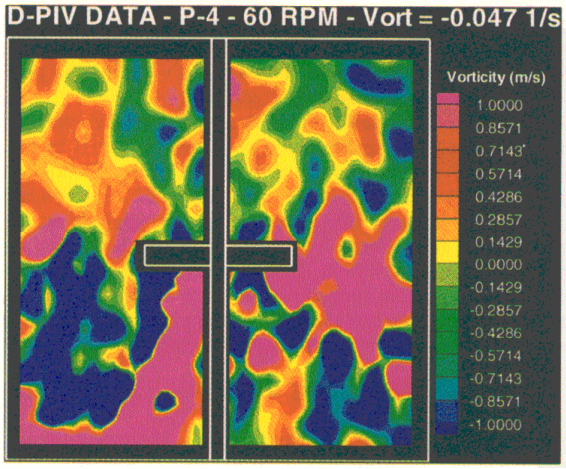

Fig. 7(*d*)

Fig. 7 Vorticity fields corresponding to the near-instantaneous DPIV velocity fields of Fig. 4

vorticity, and the flow to the left rotates counterclockwise and has a positive vorticity.

Figure 7 presents the near-instantaneous vorticity fields corresponding to the velocity fields of Fig. 4. The spatially-averaged vorticity of Fig. 7(*a*) is approximately zero because the near-instantaneous flow field is nearly symmetric (refer to Fig. 4(*a*)). The flow field of Fig. 4(*b*) is nearly symmetric, but less structured than that of Fig. 4(*a*). In this case the spatially-averaged vorticity has a relatively small magnitude, but is not zero (refer to Fig. 7(*b*)). The near-instantaneous velocity field of Fig. 4(*c*) has a large positive spatially-averaged vorticity because the large region of positive vorticity to the right of the impeller dominates the smaller region of negative vorticity to the left of the impeller (refer to Fig. 7(*c*)). Conversely, the spatially-averaged vorticity of the near-instantaneous flow field of Fig. 4(*d*) is negative because the large region of negative vorticity to the left of the impeller dominates the smaller region of positive vorticity to the right of the impeller (refer to Fig. 7(*d*)).

A portion of the time record of the spatially-averaged vorticity is shown in Fig. 8 (note that only 200 out of a total of more than 1200 seconds is shown to avoid compression of the data that obscures the oscillations between periods of positive and

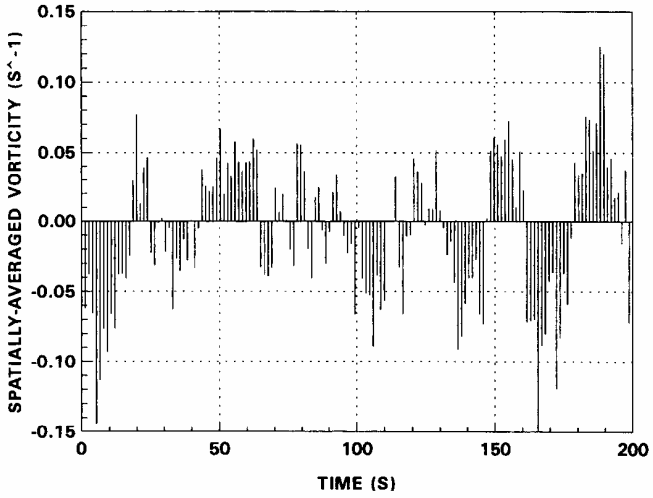

Fig. 8 Time record of the spatially-averaged vorticity of the pitched-blade turbine (C/T = 0.46)

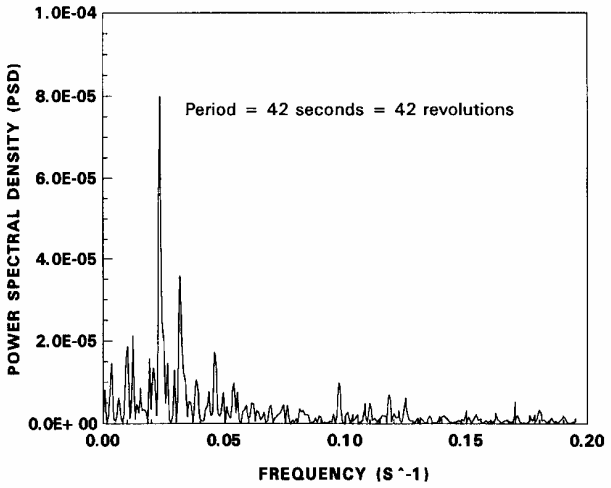

Fig. 9 Power spectral density (PSD) of the time record of the spatially-averaged vorticity of the pitched-blade turbine (C/T = 0.46)

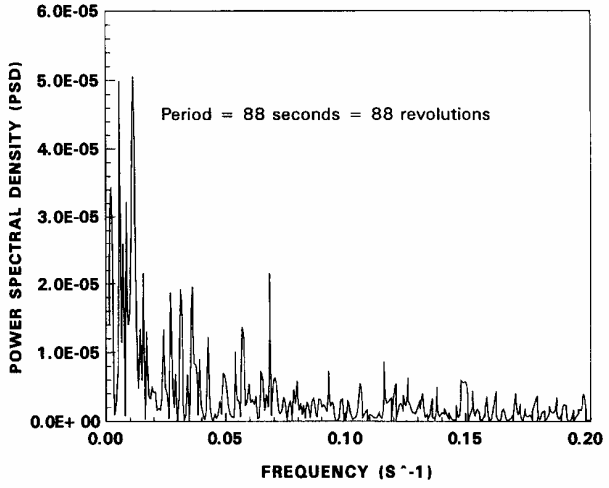

Fig. 11 Power spectral density of the time record of the spatially-averaged vorticity of the pitched-blade turbine at a lower off-bottom clearance (C/T = 0.33)

negative vorticity). Although the periods vary, including some very quick oscillations, there is a rather ordered oscillation between periods of positive spatially-averaged vorticity and periods of negative spatially-averaged vorticity.

The power spectral density (PSD) of the spatially-averaged vorticity, obtained using Fourier transforms, is shown in Fig. 9. This indicates that the dominant frequency of the fluctuations is 0.025 s^{-1} (which corresponds to a period of 40 seconds). This frequency is lower than, but of similar magnitude as, the frequencies of macro-instability of a pitched-blade turbine reported by Brůha et al. (1994, 1995). They found that the frequency of flow pattern fluctuations in water at an impeller off-bottom clearance equal to one-half of the vessel diameter (C/T = 0.5) could be correlated in the following manner.

$$f = -0.032 + 0.040N \tag{8}$$

For the impeller speed of this work (1 s^{-1}), this equation predicts a frequency of 0.008 s^{-1} (a period of 125 seconds). The disagreement between the predicted frequency and the experimental value is most likely due to extrapolation of the equation (i.e., the slower speed of this study relative to those used by Brůha et al. (1 s^{-1} relative to 3.33 to 8.33 s^{-1})). Also, the pitched-blade turbine of this study had four blades, while that used by Brůha et al. had six blades.

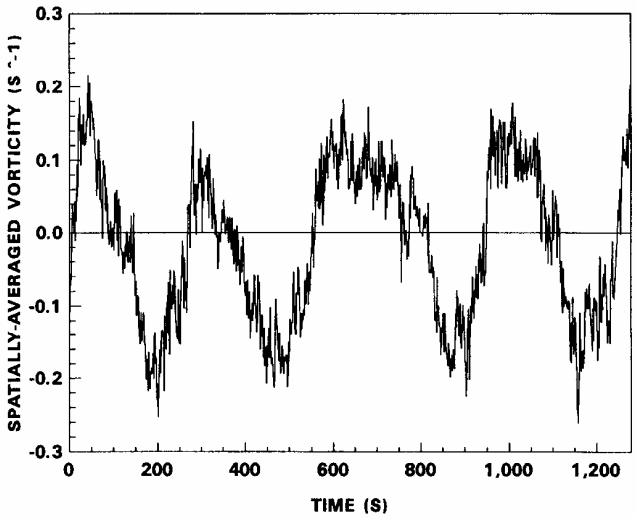

Fig. 12 Time record of the spatially-averaged vorticity of the high-efficiency impeller (C/T = 0.33)

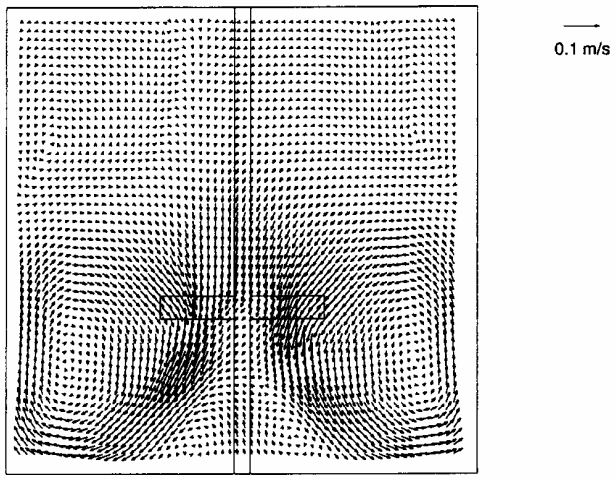

Fig. 10 Time-averaged velocity field of the pitched-blade turbine at a lower off-bottom clearance (C/T = 0.33)

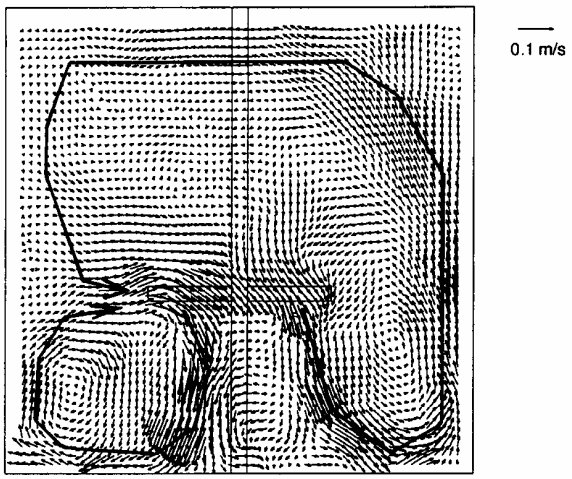

Fig. 13 Near-instantaneous velocity field of the high-efficiency impeller illustrating quick return and full circulation flow loops

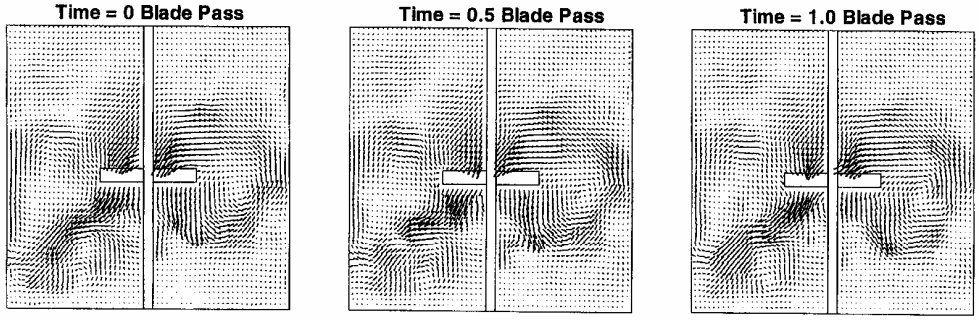

Fig. 14 Near-instantaneous velocity fields of the pitched-blade turbine taken during blade passage

The time-averaged velocity field of the pitched-blade turbine at the lower clearance ($C/T = 0.33$; also at a rotational speed of 1 s^{-1}) is shown in Fig. 10. In this instance the discharge flow reaches the base of the vessel rather than impinging on the vessel wall as was observed at the higher off-bottom clearance ($C/T = 0.46$). However, there is a small region of upflow directly below the impeller. This flow field is more typical of axial-flow impellers. The power spectral density of the spatially-averaged vorticity of the pitched-blade turbine at this lower clearance is shown in Fig. 11. In this instance, the maximum in this function is not well-defined, but peaks are found at frequencies of 0.0114 and 0.0071 s^{-1} (periods of 88 and 141 seconds, respectively). The lack of a clear maximum in the power spectral density of the spatially-averaged vorticity may indicate that the flow field of the pitched-blade turbine is more stable at the lower clearance. This would agree with visual observation of the flow and the results of Chapple and Kresta (1993). Also, these peak frequencies are more comparable to those observed by Brůha et al. (1994, 1995).

The time-averaged velocity field of the HE-3 impeller (studied at a rotational speed of 1 s^{-1} and $C/T = 0.33$), is very similar to that of the pitched-blade turbine at the lower clearance (refer to Fig. 10). However, the time-averaged velocity field of the HE-3 impeller is more axial than that of the pitched-blade turbine, with no region of upflow directly below the impeller. The time record of the spatially-averaged vorticity of the HE-3 flow field is shown in Fig. 12. This vorticity time series and the corresponding power spectral density (not shown in a figure) indicate that a very clear peak frequency occurs at 0.00301 s^{-1} (a period of 332 seconds).

The periodicity in the flow field of the HE-3 impeller is far more apparent than that of the pitched-blade impeller. The period is also much longer. As illustrated in Fig. 13, visual inspection of the near-instantaneous velocity fields of the HE-3 impeller gives insight into this phenomenon. This particular flow field can be seen to be highly asymmetric which is indicated by a large positive vorticity. In the terminology of Winardi and Nagase (1991) this flow field exhibits quick return (the short flow loop below and to the left of the impeller) and full circulation (the long flow loop to the right of the impeller that crosses the top of the vessel and returns to the upper left of the impeller). Visual observation of the flow indicates that this flow asymmetry is very persistent, if not permanent, and slowly precesses around the vessel.

Blade Passage Effects

A concern that arises when studying transient phenomena in agitated vessels is the effect of blade passage on the flow field. Since the periods of the transients observed in this study are much longer than those associated with blade passage, it is unlikely that the transients are due to blade passage. However, if the asymmetry in the flow fields would arise from the high frequency blade passage, they might still show up as low frequencies in the current measurements due to aliasing. To experimentally validate that the observed asymmetries are not related to blade passage, near-instantaneous velocity fields were obtained with the pitched-blade turbine ($C/T = 0.46$) during blade passage through the plane of study (this requires a significantly faster sampling frequency than used in the preceding analysis). Three of these velocity fields taken during one blade passage are shown in Fig. 14. Although there are minor differences in the flow fields, it is apparent that blade passage does not strongly influence the asymmetries present in the flow field.

Conclusions

Comparison of DPIV and LDV velocity fields indicates that digital particle image velocimetry is a reliable technique for studying flow in agitated vessels. A novel application of DPIV to the study of instability in the flow fields produced by a pitched-blade turbine and a high-efficiency impeller illustrates the further potential of the DPIV technique. Specifically, time series analysis of the spatially-averaged vorticity of the flow fields of these impellers indicates that transients with time scales corresponding to forty to over three hundred impeller revolutions are present. Further, these transients were found to not depend on impeller blade passage. These results have important implications for computational modeling because descriptions of agitated vessels that are based on time-averaged flow fields with superimposed turbulence may not accurately capture the mixing associated with these low-frequency phenomena. Future studies will include further characterization of the transients, specifically the influence of impeller type, system geometry, and operating conditions. It is also critical that the origins of the transients and their influence on mixing performance, subjects that have previously received little attention, be the focus of future work.

Acknowledgments

We would like to thank Cassian Lee of The Dow Chemical Company for providing the LDV data of Figs. 2 and 3. Also, we acknowledge the assistance of Julian B. Fasano and James W. Nordmeyer of Chemineer, Inc. in the completion of this work.

References

Bakker, A., and Van den Akker, H. E. A., 1994a, "Single-Phase Flow in Stirred Reactors," *Trans IChemE*, Vol. 72, Part A, pp. 583–593.

Bakker, A., and Van den Akker, H. E. A., 1994b, "Gas-Liquid Contacting with Axial Flow Impellers," *Trans IChemE*, Vol. 72, Part A, pp. 573–582.

Brůha, O., Fořt, I., and Smolka, P., 1994, "Flow Transition Phenomenon in an Axially Agitated System," *Proceedings of the Eighth European Conference on Mixing* (IChemE Symposium Series Number 136), pages 121–128, Cambridge, United Kingdom, Sept. 21–23.

Brůha, O., Fořt, I., and Smolka, P., 1995, "Phenomenon of Turbulent Macro-Instabilities in Agitated Systems," *Collect. Czech. Chem. Commun.*, Vol. 60, pp. 85–94.

Chapple, D., and Kresta, S., 1993, "The Effect of Geometry on the Stability of Flow Patterns in Stirred Tanks," paper presented at Mixing XIV, Santa Barbara, California, June 20–25.

Fasano, J. B., and Bakker, A., 1993, "Particle Image Velocimetry: 2-D Velocity Fields for Agitated Tanks for the Six Bladed Disc and the Four Bladed 45° Pitched Impellers," paper presented at Mixing XIV, Santa Barbara, CA, June 20–25.

Haam, S., Brodkey, R. S., and Fasano, J. B., 1992, "Local Heat Transfer in a Mixing Vessel Using Heat Flux Sensors" *Industrial and Engineering Chemistry Research,* Vol. 31, No. 5, pp. 1384–1391.

Kresta, S. M., and Wood, P. E., 1993, "The Mean Flow Field Produced by a 45° Pitched Turbine: Changes in the Circulation Pattern Due to Off Bottom Clearance," *Canadian Journal of Chemical Engineering,* Vol. 71, pp. 42–53.

Lee, C., 1994, private communication with A. Bakker.

Press, W. H., Teukolsky, S. A., Vetterling, W. T., and Flannery, B. P., 1992, *Numerical Recipes in Fortran: The Art of Scientific Computing,* Cambridge University Press.

Wang, M.-H., Calabrese, R. V., and Bakker, A., 1995, "Effect of Reynolds Number on the Flow Generated by Pitched Blade and High Efficiency Turbines," presented at Mixing XV (15th Biennial North American Mixing Conference) Banff, Alberta, Canada, June 18–23.

Willert, C. E., and Gharib, M., 1991, "Digital Particle Image Velocimetry,' *Experiments in Fluids,* Vol. 10, pp. 181–193.

Winardi, S., and Nagase, Y., 1991, "Unstable Phenomenon of Flow in a Mixing Vessel with a Marine Propeller," *Journal of Chemical Engineering of Japan,* Vol. 24, No. 2, pp. 243–249.